Journal of Applied Polymer Science

Evaluation of a novel profile control agent for enhancing an oil-recovery application

Wanfen Pu,[1,2] Cailin Wen,[1,2] Rui Liu,[1,2] Fayang Jin,[1,2] Chongyang Wang,[1,2] Zhicheng Liao[3]

[1]School of Petroleum and Gas Engineering, Southwest Petroleum University, Chengdu 610500, Sichuan, China

[2]State Key Laboratory of Oil and Gas Reservoir Geology and Exploitation, Southwest Petroleum University, Chengdu 610500, Sichuan, China

[3]Chuanxi Drilling Company, Chuanqing Drilling Engineering Company, Limited, China National Petroleum Corporation, Chengdu 610015, Sichuan, China

Correspondence to: C. Wen (E-mail: wclwendy210@163.com)

ABSTRACT: In this study, a kind of novel profile control agent, polymer/montmorillonite composite particle (PMCP), which was prepared by an *in situ* intercalative polymerization method involving rubbers and a hydrophobic monomer (HM), was provided with the aim to modify the injection profile for enhancing oil recovery. The chemical structure of the PMCP was characterized by Fourier transform infrared spectroscopy and X-ray diffraction, respectively. The results prove that the intercalation effect occurred between the polymer and montmorillonite. The swelling properties of the PMCP was studied under harsh reservoir conditions as a function of the aging time to determine the effect of rubbers and HM. The toughness of the optimal particle was investigated by a maximum pressure method followed by core experiments to evaluate the injection and profile improvement performance. The data indicated that PMCP-4 containing the rubber of nitrile butadiene rubber and HM showed advanced properties, such as the swelling ratio, heat resistance, salinity tolerance, and water retention, compared to the other PMCPs. Moreover, the PCMP also exhibited superior toughness, injectivity, and profile control ability. Therefore, PMCP-4 is a promising profile control agent, especially in fractured formations with harsh conditions. © 2016 Wiley Periodicals, Inc. J. Appl. Polym. Sci. **2016**, *133*, 43756.

KEYWORDS: addition polymerization; adsorption; rubber; X-ray

Received 28 October 2015; accepted 8 April 2016

DOI: 10.1002/app.43756

INTRODUCTION

In stratified, fractured, or extensively water-flooded oil reservoirs, the oil-recovery efficiency tends to be very low because the displacing fluid would flow mainly thought the most permeable regions, leaving a large amount of crude oil untouched.[1] Given this issue, deep profile modification techniques on injector wells have already been attempted with the aim of controlling the heterogeneous permeability profile to raise the oil-recovery magnitude. As one mature technique, polymer gels have been studied extensively to treat the in-depth permeability for fractured reservoirs.[2–6] However, some drawbacks, such as a weak salt tolerance and temperature resistance, low strength, nonselective injection, and blocking, significantly limit their wide application in reservoirs with harsh condition. On the other hand, microbially enhanced oil-recovery techniques, which probably can considerably increase oil production in high-permeability reservoirs because of their insensitivity to salinity and temperature, seem not to have very high potential because of the well plugging problem, even though they have been successfully applied in some oil fields.[7,8]

Acrylamide (AM) and acrylic acid (AA) monomers that are polymerizable are the raw materials of polyacrylamide. In other words, polyacrylamide can be synthesized through homopolymerization or copolymerization reactions of AM and AA, which are widely used in the Daqing Oil Field. Meanwhile, AM[9,10] and AA,[11] with superior hydrophilicities, have been used to develop hydrophilic, preformed particle gels with added crosslinking agent. In this case, lots of acylamino and carboxyl groups existed in the molecules of the preformed particle gels and contributed to water absorption. As an alternative, the preformed particle gels, which showed good water swelling, elasticity, deformability,[12] and resistance to salinity and temperature,[13,14] have attracted more and more research interest for in-depth profile modification for fractured reservoirs. They are formed at surface facilities before they are injected into the reservoir; this can eliminate the effect of adsorption and shear degradation compared with *in situ* gels.[15]

© 2016 Wiley Periodicals, Inc.

Preformed particle gels are three-dimensional, hydrophilic polymers that can swell in water but do not dissolve in it, whereas their volumes vary with the temperature, salinity, and pH change.[16–18] With Tahe Oil Field (Tarim Basin, China) as an example, this oil field is a typically fractured reservoir with a high temperature (120 °C) and high salinity (220,000 mg/L). In this case, many more stable particle gels are required to resist the salt, temperature, and mechanical degradation. Sang *et al.*[16] investigated the water absorption properties of a branched, preformed particle gel, but the reservoir conditions (70 °C and 19,334 mg/L) were gentle and not as harsh as those in the Tahe Oil Field. Bai[19] indeed studied the acceptance of all kinds of salts and concentrations under a temperature of 110 °C, but there was a still 10 °C difference to 120 °C. To achieve the high salt- and temperature-resistance properties, efforts in nanocomposites have been made in recent decades; these studies have provided great progress on the profile modification technique.[20] Montmorillonites (MMTs) were introduced to the system to increase the strength of the gel particle because of their intercalation properties; this enhanced the tolerance of the particles to the temperature and salinity,[21–23] However, it is still challenging for the particles in reservoirs having temperatures above 100 °C and salt concentrations above 100,000 mg/L.[24] Some composites have even shown a dramatic increase in the postdegradation gel viscosity; when nanoclay was added, however, they showed a temperature resistance of just 80 °C and a salt concentration of 10,000 mg/L.[25]

To promote the water retention of particle gels under such harsh conditions, hydrophobic monomers (HMs) could be considered as a supplement. Typically, hydrophobically associating polymers have good salt tolerance and shear resistance because of the addition of HM. Several widely applicable HMs are listed here; the first one is long-chain alkyl HM. Long-chain alkyl, which is found in its hydrophobic unit, can link to allyl, acylamino, or alcyl. The typical long-chain alkyl hydrophobically associating polymer was prepared by the free-radical polymerization[26] of long-chain alkyl HM. The second one is double-tailed HM. It has two hydrophobic hydrocarbon chains; this enhanced the density of the hydrophobic side chains in the copolymer. Its polymer shows superior hydrophobic associating properties.[27] The third one is benzenoid HM. The introduction of a rigid benzene ring into the hydrophobic chains not only improves the temperature resistance of the polymer but also restrains the hydrolyzation of acyl amid; this contributes to the long-time stability of polymer. The voluminous benzene ring enhances the hydrophobic chain's rigidity, making it easily stretch. Therefore, this kind of HM shows preferable hydrophobically associating properties and better viscosity.[28] The last one is double-tailed HM with a benzene ring. The novel double-tailed AM hydrophobically associating polymer is characterized by a double-tailed structure and benzene ring structure together. It shows excellent viscosity-promoting properties and preferable temperature resistance (80 °C) and salt tolerance (100,000 mg/L).[29]

In addition, to improve the particle's migration capabilities under harsh conditions, soft diverting agents making up the aromatic monomer show long-time stability and good deformability;[30] this is a novel technology in profile control to overcome high-temperature and high-salinity conditions. Therefore, soft agents must be used as the material when particle gels are prepared. It is known that the polymer has a shorter validity and weak scouring resistance, whereas rubber has excellent elasticity and shear resistance. The addition of rubber into the polymer system could overcome the disadvantages of the polymer.[31] Generally, varieties of rubbers are alternative, such as chloroprene rubber, nitrile–butadiene rubber (NBR), styrene–butadiene rubber (SBR), natural rubber, and polydimethylsiloxane rubber. The recombination between rubbers and adsorbent resins (polyacrylamide, cellulose, or sodium polyacrylate) could synthesize water-swellable materials. Wang *et al.*[32] studied a kind of amphiphilic poly(ethylene oxide)-*b*-poly(butyl acrylate) based on the blending of a natural rubber matrix with crosslinked sodium polyacrylate. The results show that the greater the amount of crosslinked sodium polyacrylate resin was, the higher the swelling ratio of the rubber was. Dehbari *et al.*[33] investigated the effects of polydimethylsiloxane rubber and poly(acrylic acid) partially neutralized by sodium hydroxide (NaOH) on a novel water-swellable rubber; the results indicate that the water-swelling ability and durability of the water-swellable rubber composites further improved when rubber and NaOH were added together. However, NBR and SBR had more advantages than the rubbers mentioned previously; these included a low cost, good thermostability, and superior shear resistance, and this made them suitable soft agents for preparing composite materials in high-temperature and high-salinity conditions.[34,35]

Because the current particle technology dealing with high-temperature and high-salinity reservoirs is more or less defective, in this study, we developed a novel polymer/montmorillonite composite particle (PMCP) that could be used in deep displacement for such reservoirs. Here, a PMCP was mainly prepared by the blending of AM and AA as superabsorbent resins, NBR and SBR as rubber matrixes, HM as the hydrophobic agent, and MMT as a reinforcement agent. The key mechanisms in the PMCP were as follows:

1. The combination between the MMT and organic monomers rendered PMCP with toughness and strength under high-temperature and high-salinity conditions.
2. The collaboration of rubbers and HM equipped the particle with enhanced toughness and strength because of the inertial properties of the rubber.
3. The formed hydrophobic micro area of the HM improved the particle's salinity resistance and thermostability.

Fourier transform infrared (FTIR) spectroscopy and X-ray diffraction (XRD) were conducted to characterize the structure of the synthesized particle. In addition, the swelling properties were evaluated under different temperatures (60, 80, 100, and 120 °C) and salinities (0, 55,000, 110,000, 165,000, and 220,000 mg/L) as a function of the aging time to examine the effect of the components. Eventually, the toughness, injectivity, and profile improvement performance of the optimal particle were investigated via a toughness assessment experiment and core experiment. We expect that the optimal particle will be applicable for profile modification in fractured oil fields, especially those with high temperatures and high salinity.

EXPERIMENTAL

Materials

Sodium MMT (200 mesh, 1.7 g/cm^3) was purchased from Zhejiang Feng Hong New Material Co., Ltd which was the optimal material in early study.[36] The superabsorbent resin (AM, 99.0%,

Table I. Grades of Rubber Emulsion Products

Product	Solid content (%)	Viscosity (mPa s)	pH	Particle size (nm)	Surface tension (mN/m)
NBR	43.0	30.0	8.00	80	25.0
SBR	35.0	20.0	8.00	80	50.0

The properties were measured at 25 °C, and the two rubber emulsion products appeared milk white. The contents of acrylonitrile and bonded styrene were 32 and 23.5%, respectively, in the NBR and SBR solids.

and AA, 99.5%), neutralization agent (NaOH, 98%), *N,N′*-methylene bisacrylamide crosslinking agent ($C_7H_{10}N_2O_2$; 98.5%), and initiator [$(NH_4)_2S_2O_8$, 98%, and $NaHSO_3$, 58.5%] were supplied by Chengdu KeLong Chemical Reagent Co., Ltd. (China). The emulsion products of NBR and SBR (grades shown in Table I) were purchased from Zibo Qilong Chemical Co., Ltd. (China). HM (98%)[37] was prepared in our laboratory according to the structural formula shown in Figure 1; it contained a polymerizable carbon–carbon double bond, hydrophobic long-chain alkyl, and hydrophilic acylamino and sulfonic group. It showed the properties of temperature resistance and salt tolerance. Meanwhile, simulated formation water with a high salinity (220,000 mg/L, Xidaliya Oil Fields, Xinjiang, China) was prepared in laboratory, and the chemical composition of the simulated formation water is listed in Table II.

Preparation of PMCP

As shown in Table III, there are four kinds of PMCPs (PCMP-1, PCMP-2, PCMP-3, and PCMP-4). With PCMP-2 as an example to explain the detailed procedure of preparation. First, 6.67 g of AM and 1.92 mL of AA monomer were predissolved in distilled water, and then, 1.67 g of the SBR sample was added continuously to the reaction mass. This was followed by the mixture of 0.01 g of HM. We noted that all of the reaction systems were adjusted to pH of 7 with NaOH solution (1 wt %). Afterward, 20 g of MMT was slowly added to the system and stirred at room temperature (25 °C) until a homogeneous polymer suspension was formed. The MMT was adequately intercalated with an organic monomer after about 2 h. The crosslinking agent and initiator were then added into the solutions; they were then vibrated with an ultrasonic wave (KH3200, Kun Shan He Chuang Ultrasonic Instruments Co., Ltd., China). Finally, the polymer gel samples were kept at 50 °C in a water bath kettle for 4–6 h. The four samples were cut into small pieces, dried at 80 °C for 24 h, and smashed into particles for further utilization.

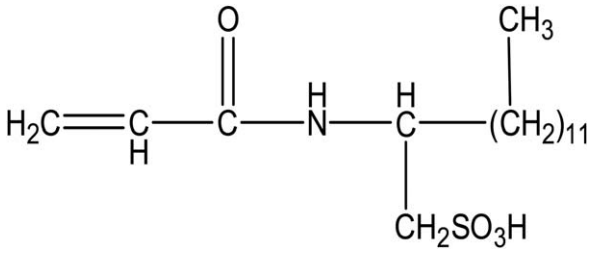

Figure 1. Chemical structure of the HM.

Characterization

FTIR spectroscopy was carried out with an instrument from Beijing Ruili Analysis Instrument Co., Ltd., with KBr pellet in the range 4000–500 cm^{-1}. The characteristic peaks were recognized when we analyzed the function groups in PMCP; these intensities were divided into five grades: vs, very strong; s, strong; m, middle strong; w, weak; and vw, very weak. ν and δ corresponded to the stretching and bending vibrations, respectively. The XRD patterns were recorded with an X'Pert Pro diffractometer (PANalytical, The Netherlands) equipped with an X'Celerator detector and with Kα radiation (40KV, 30 mA). The layer spacing was calculated according to the Bragg equation:

$$n\lambda = 2d \sin \theta$$

where λ is the wavelength of the X-ray beam (0.154 nm), θ is the diffraction angle,[38] and n is the diffraction series, which was equal to 1 here. Typically, the samples of PMCP-2 and PMCP-4 were subjected to FTIR spectroscopy and XRD characterization, and the samples were smashed into fine powders before characterization.

Swelling Performance

Typically, 1 g of the PMCP sample was loaded into a sieve with a mesh of 32 and, then, merged into 40 mL of simulated formation water with a salt concentration ranging from 0 to 220,000 mg/L. Each test was conducted under a temperature ranging from 60 to 120 °C, respectively. Along with the aging time, the swelling particle was weighed, and the particle swelling ratio (M) was calculated. This ratio is considered as the most important parameter in the evaluation of the particle performance in high-temperature and high-salinity reservoirs. It can can be calculated by the following expression:

$$M = (W_t - W_0)/W_0 \quad (1)$$

where W_t is the weight of the particle at aging time t and W_0 is the initial weight (1 g). The optimal particle was selected by the evaluation of the PMCP's performance with respect to salt tolerance, temperature resistance, and water retention by the following:

1. Evaluation of the salt tolerance: When the PMCP was in complete expansion, we analyzed its swelling ratio under a temperature of 120 °C and at different salt concentrations from 0 to 220,000 mg/L.
2. Evaluation of the temperature resistance: When the PMCP was in complete expansion, we analyzed its swelling ratio

Table II. Composition of the Xidaliya Formation Water

Oil field	$CaCl_2$ (mg/L)	NaCl (mg/L)	$MgCl_2{\cdot}6H_2O$ (mg/L)	$MgCl_2$ (mg/L)	Gross (mg/L)
Xidaliya	29,530.1	172,542.3	11,151.2	6780.1	220,003.7

Table III. Compositions of the PMCP Samples

Sample	AM (g)	AA (mL)	MMT (g)	SBR (g)	NBR (g)	HM (g)	Distilled water (g)	$C_7H_{10}N_2O_2$ (g)	$(NH_4)_2S_2O_8$ (g)	$NaHSO_3$ (g)	pH
PMCP-1	6.672	1.92	20.002	1.672	—		33.331	0.812	2.111	1.116	7.01
PMCP-2	6.675	1.93	20.011	1.671	—	0.012	33.342	0.815	2.130	1.113	7.12
PMCP-3	6.669	1.91	20.013	—	1.673		33.351	0.819	2.118	1.114	7.04
PMCP-4	6.671	1.92	20.005	—	1.672	0.011	33.329	0.814	2.127	1.121	7.09

The mass ratio of AM to AA was 3.5:1, and the mass ratio of $(NH_4)_2S_2O_8$ to $NaHSO_3$ was 1.9:1. The proportions of the rubber, HM, distilled water, and $C_7H_{10}N_2O_2$ were 2.5, 0.01, 49, and 1.2%, respectively.

under a salt concentration of 220,000 mg/L and at different temperatures from 60 to 120 °C.

3. Evaluation of the water-retention capability: The water-retention rate was considered as the index of the long-time thermal stability and profile control capability. After the salt tolerance and temperature resistance was investigated, we chose the previous completely swollen PMCPs under 120 °C and 220,000 mg/L, put them under the same conditions for 2 months, and calculated the water-retention rate (N_P) at different aging times as follows:

$$N_p = (W_t / W_P) \times 100\% \quad (2)$$

where W_P is the completely swollen weight.

Toughness Assessment Experiment

The measurement of the particle's strength and toughness were performed with the maximum pressure method at room temperature (25 °C), the experiment was conducted by a constant flow pump (HLB-1040), which was purchased from Dongtai Yanshan Instrument Factory (Jiangsu, China). One gram of PMCP with a particle size of 0.5 mm was kept under the same experimental conditions (salt concentration and temperature) to evaluate the swelling performance. After full expansion, the swollen particle was poured into a stainless steel tube (the diameter of the sieve pore was 1.7 mm) and then injected with the same flow controlled by the pump to make the piston exert pressure on the tube. Under the force of the piston, the particle

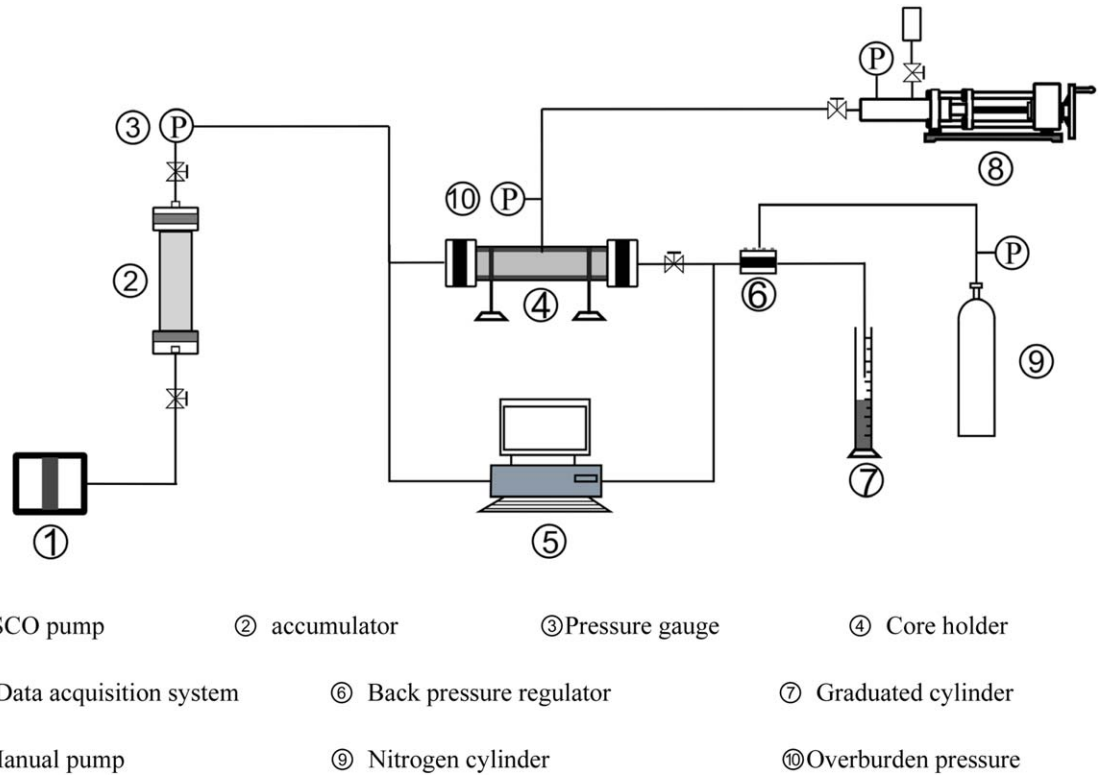

Figure 2. Schematic diagram of the single-core experimental setup: (1) Isco pump, (2) accumulator, (3) pressure gauge, (4) core holder, (5) data-acquisition system, (6) back-pressure regulator, (7) graduated cylinder, (8) manual pump, (9) nitrogen cylinder, and (10) overburden pressure. [Color figure can be viewed in the online issue, which is available at wileyonlinelibrary.com.]

Table IV. Profile Control Performance of the Particle in Different Permeability Contrast Cores

Group	Core sample	Permeability contrast	Fracture width (cm)	Permeability (μm^2)		Selective injection (PV)	Ratio of water absorption (%/%)		η (%)
				K_b	K_a		Q_{hb}	Q_{ha}	
1	1	6.08	0.07	1.12	0.93	0.12	87/13	15/85	97.4
	2		0.28	6.81	0.05	0.88			
2	3	9.03	0.06	0.79	0.67	0.04	93/7	10/90	99.2
	4		0.75	7.13	0.02	0.96			

passed through a steel-wire screen 1 mm in diameter, and the maximum pressure (P_{max}) was measured in the process. This represented the strength of the particle. This procedure was repeated after the particles were completely passed through the screen, the maximum pressure in the second trial (P_{max}') was also measured. The toughness coefficient (f) was, therefore, calculated with the following equation:

$$f = P'_{max} / P_{max} \quad (3)$$

Core Experiment

Single-Core Experiment. In this study, a single-core experiment was first conducted to evaluate the injectivity of the particle in the real formation. The artificially fractured carbonate core (core size: length = 7.025 cm, diameter = 3.76 cm, fracture

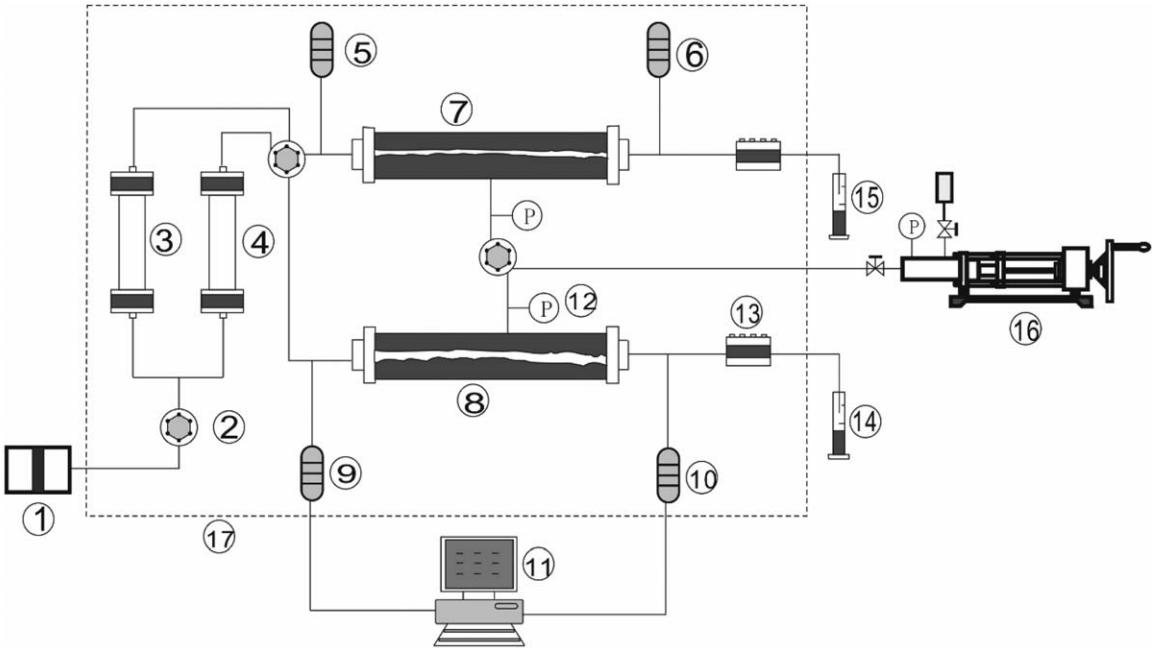

Figure 3. Schematic diagram of the double-parallel-core equipment: (1) Isco pump, (2) six-way valve, (3) brine, (4) suspension, (5) input pressure sensor, (6) output pressure sensor, (7) core holder for low-permeability fractured core, (8) core holder for high-permeability fractured core, (9) input pressure sensor, (10) output pressure sensor, (11) data acquisition system, (12) overburden pressure, (13) back-pressure regulator, (14) graduated cylinder, (15) graduated cylinder, (16) manual pump, and (17) oven thermostat.

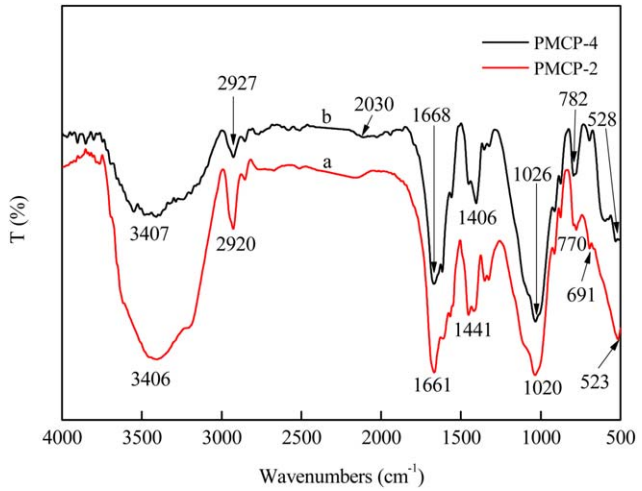

Figure 4. FTIR spectra of (a) PMCP-2 and (b) PMCP-4. [Color figure can be viewed in the online issue, which is available at wileyonlinelibrary.com.]

width = 2 mm, height = 3.5 mm) was used to stimulate the fractured vuggy formation, and a particle suspension with a mass fraction of 0.3 wt % of the particle and a swollen size of 4 mm was also prepared. The experimental setup is depicted in Figure 2. The core was assembled in the setup with a overburden pressure of 13 MPa and then pressurized at a constant of 10 MPa with a back-pressure regulator to reproduce the reservoir conditions. All of the injectants were injected at a constant velocity of 5 mL/min with the pump. During this process, the pressure difference variation versus particle migration in the core was recorded, and the effluent was also quantified with a graduated cylinder. Thus, the resistance factor (R_F) of the particle was calculated with the following formula:

$$R_F = \lambda_w/\lambda_p = (K_w/\mu_w)/(K_p/\mu_p) \quad (4)$$

where λ_w is the mobility of the brine solution, λ_p is the mobility of the particle solution, K_w is the core's permeability with the brine flooding, K_p is the core's permeability with the particle flooding, and μ_w is the viscosity of brine solution, μ_p is the viscosity of the particle.

According to the Darcy formula, the core permeability (K; K_w or K_p) can be expressed with the following equation:

$$K = (Q\mu L)/(A\Delta P) \quad (5)$$

where Q is the flow rate of the displacing phase as the value is 5 mL/min, μ is the viscosity of the displacing phase, L is the length of the core, A is the cross-sectional area of fracture, and ΔP is the pressure difference of the injection displacing phase.

A combination of eqs. (4) and (5) gives

$$R_F = \Delta P_p/\Delta P_w \quad (6)$$

where ΔP_p is the pressure difference of the injection particle solution and ΔP_w is the initial pressure difference of the injection brine solution.

Double-Parallel-Core Experiment. Double-parallel-core experiment was performed to evaluate the ability of optimal particles entering and blocking the fractures. Two groups of artificial fractured cores with significant permeability contrast were prepared, as listed in Table IV, and then, we assembled them into the core holders, as illustrated in Figure 3. The procedure described as follows used for the double-parallel core.

1. The tightness of the devices was checked with brine solution.
2. The relative water absorption of the large and small fractures was measured during brine injection, and subsequently, the permeability of the cores before profile control was calculated.
3. The injection of the 1.0 pore volume (PV) of the particle suspension into the parallel cores with the velocity of 5 mL/min and measurement of the selective injection of the profile control agent on the two cores.
4. The cores were discharged from the core holder and then sealed. After 24 h of aging in an oven at 120 °C, the cores were reassembled in the experimental setup, as shown in Figure 3. Brine was injected to flood the cores and to measure the relative water absorption. The permeability and profile improvement rate values of the cores after profile control were determined. The profile improvement rate (η) was calculated with the following equation:

$$\eta = (Q_{hb}/Q_{1b} - Q_{ha}/Q_{1a})/(Q_{hb}/Q_{1b}) \times 100\% \quad (7)$$

where Q_{hb} and Q_{ha} are the water absorptions in the high-permeability core before and after profile control, respectively. Similarly, Q_{1b} and Q_{1a} are the water absorption in the low-permeability core before and after profile control, respectively. The higher the profile improvement rate is, the better the profile control agent performance is.

RESULTS AND DISCUSSION

Characterization

FTIR Analysis. The FTIR spectra of PMCP-2 and PMCP-4 are shown in Figure 4. The two spectra presented similar patterns. For PMCP-2 and PMCP-4, the peaks from FTIR spectroscopy (ν/cm^{-1}) can be expressed as follows: 3407 cm^{-1} [vs, ν(O—H)], 1661 cm^{-1} [s, ν(C=C); s, δ(N—H)], 2920 cm^{-1} [w, δ(C—H)], 1441 cm^{-1} [s, ν(C—C)], 1353 cm^{-1} [w, ν(C—N)], 1317 cm^{-1} [w, ν(S=O)], 1020 cm^{-1} [s, ν(S—O)], 770 cm^{-1} [s, δ(N—H)], and 523 cm^{-1} [s, δ(Si—O—Si)]. The only difference was that PMCP-2 and PMCP-4 presented different characteristic peaks: 691 cm^{-1} [w, δ(C—H)] for PMCP-2 and 1353 cm^{-1} [w, ν(C≡N)] for PMCP-4. The aforementioned peaks included —COOH, —$CONH_2$, —SO_3H, —CH_2—, and Si—O aromatic and nitrile groups; this indicated a combination of organic materials and MMT. The FTIR characterization results demonstrate that the PMCP was the copolymerization product of all of the reactants; the rubbers and HM were effectively introduced because of the strong hydrogen bonding between the MMT, AM, and rubber.

Table V. Layer Spacing of the Samples

Sample	MMT	PMCP-2	PMCP-4
2θ	5.865	4.233	4.352
d (nm)	1.505	2.085	2.028

XRD Analysis. XRD characterization was also conducted for MMT, PMCP-2, and PMCP-4, respectively. Table V lists the diffraction angle and layer spacing of the three samples. Figure 5 displays the diffraction patterns of MMT, PMCP-2, and PMCP-4. As depicted, the diffraction angle of MMT was observed at a 2θ of 5.865°, and thus, the original layer spacing calculated for MMT was 1.505 nm. Compared with MMT, the layer spacing of PMCP-2 and PMCP-4 were expanded by 0.58 and 0.523 nm, respectively, because of the insertion of organic monomer into the interlayer of MMT. The XRD characterization of typical particles showed that the layer spacing of the modified MMT was expanded by approximately 0.5–0.6 nm; this was in agreement with our anticipation of the intercalation of organic material into inorganic material.

The microstructure of the polymer/MMT[39] is depicted as Figure 6; the straight lines and curves represent the MMT and polymer, respectively. The polymer was not only mixed with MMT but was also inserted into the lamella of the MMT; this led to the significant expansion of the layer spacing. In addition, the MMT remained in the initial direction with the particular order. The layer mineral MMT is usually used for intercalative polymerization in the preparation of composite materials. The polymer interacts with MMT on the basis of the chemical interaction between the sufficient hydroxyl on the MMT's surface with the organic polymer. The Na^+ of MMT is easily replaced by most of the organic cationic; this contributes to the expansion of the layer spacing. Additionally, the good compatibility between the MMT and the polar monomers of AM and rubber leads the polymer to enter the MMT lamella because the polar monomers have a positive effect on the exfoliation of MMT in poly(methyl methacrylate)-*co*-poly(acrylic acid)/MMT.[40] Meanwhile, the internal swelling properties of the polymers make the layer spacing increase further.

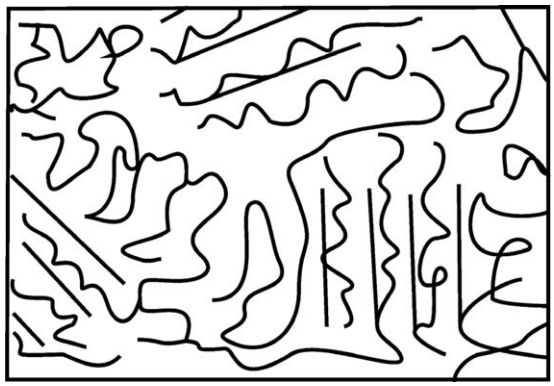

Figure 6. Schematic of the interaction in the polymer/MMT composite.[26]

Evaluation of the Swelling Performance

Evaluation of the Salt Tolerance. Figure 7 shows that the salt concentration greatly influenced the swelling ratio, higher salt concentration, lower swelling ratio, and relationship between salt concentration, and the swelling ratio was mainly divided into two areas:

1. The first area showed the swelling ratio rapidly declined with increasing salt concentration. As the swelling ratio decreased from 16 to 8 under salt concentrations ranging from 0 to 55,000 mg/L.
2. The second area showed that the swelling ratio was not affected by the salt concentration with the swelling ratio maintained at 6–8 with the salt concentration ranging from 55,000 to 220,000 mg/L

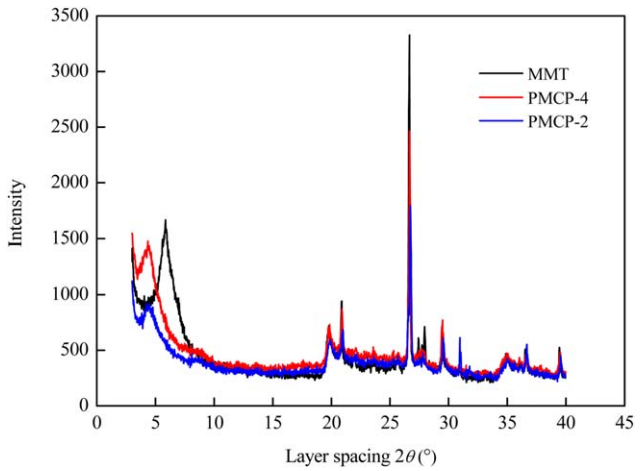

Figure 5. XRD patterns of MMT, PMCP-2, and PMCP-4. [Color figure can be viewed in the online issue, which is available at wileyonlinelibrary.com.]

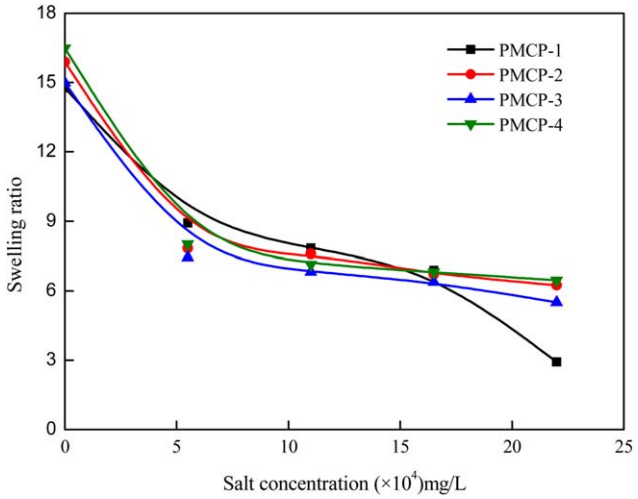

Figure 7. Effect of the salt concentration on the swelling ratio. [Color figure can be viewed in the online issue, which is available at wileyonlinelibrary.com.]

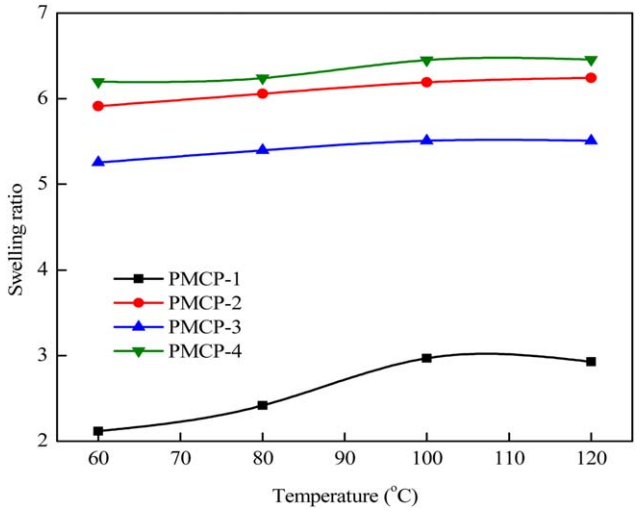

Figure 8. Effect of the temperature on the swelling ratio. [Color figure can be viewed in the online issue, which is available at wileyonlinelibrary.com.]

3. When PMCP-1 displayed the third area, in which the swelling ratio quickly decreased under a salt concentration ranging from 165,000 to 220,000 mg/L. It presented a bad swelling ratio at 220,000 mg/L. Additionally, in same salinities, the swelling ratio of PMCP-2 was greater than that of PMCP-1; likewise, the swelling ratio of PMCP-4 was greater than that of PMCP-3. One reasonable interpretation was that the water-soluble sulfonic group of HM was insensitive to cations, and this benefited the tolerance to high salinity. Thus, PMCP (PMCP-2, PMCP-3, PMCP-4) had a good salt tolerance at 220,000 mg/L.

Evaluation of Temperature Resistance. As shown in Figure 8, the swelling ratio obviously increased with temperature; this could be explained by the fact that the temperature contributed to the acceleration of molecular thermal motion; hence, the bonding force between the molecules were weakened at high temperatures. For PMCP-1, all swelling ratios were just 2 at 220,000 mg/L; this might have been because the molecular bond of SBR easily broke under high temperatures and high salt concentrations. Thus, PMCP-1 was not suitable to act as a profile control agent for objective reservoirs. We noticed that PMCP-2 showed good temperature resistance when the HM was added; all the swelling ratios were greater than those of PMCP-1 at 220,000 mg/L. It was evident that HM protected the particle from dissolution in water at high temperatures. PMCP-3 and PMCP-4 displayed the same swelling performance as PMCP-2; however, it was clear that the difference was that the swelling ratio of PMCP-4 was slightly higher than those of the other two. It was 6.5 at 120 °C and 220,000 mg/L; the thermostability of NBR was better than that of SBR. In all, the PMCPs (PMCP-2, PMCP-3, PMCP-4) showed excellent temperature resistance at 120 °C.

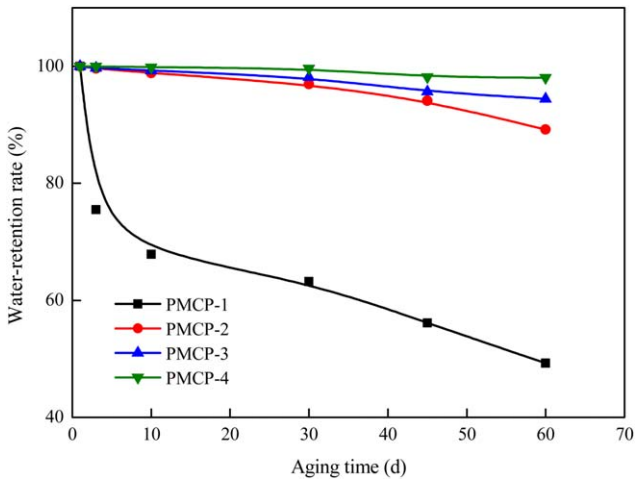

Figure 9. Water-retention capability of PMCP at 120 °C. [Color figure can be viewed in the online issue, which is available at wileyonlinelibrary.com.]

Evaluation of the Water-Retention Capability. Figure 9 shows the results of the water-retention capability in 60 days, and the water-retention rate of PMCP decreased over time. PMCP-2, PMCP-3, and PMCP-4 showed good water-retention rates, which were above 89% at different aging times, whereas PMCP-1 displayed severe dehydration when its water-retention rate sharply decreased. PMCP-4 presented a higher water-retention rate than PMCP-2 and PMCP-3; this reached to 98% after 60 days. In addition, it retained a good toughness and strength after the experimental process. This demonstrated the excellent water-retention capability of PMCP-4. The reason why PMCP-4 possessed good water-retention capability could be explained as follows:

1. Under the effect of tiny MMT, the outer space of the micro-network structure got tighter. It also indicated the strong force between the MMT and organic monomers.
2. The heat resistance of NBR was superior to SBR.
3. The formed hydrophobic micro area of HM improved the particle's thermostability.

For HM, the water-soluble sulfonic group was insensitive to cations and benefited the tolerance to high salinity. Also, the long alkyl chain was hydrophobic. When HM was introduced into the composite, the hydrophobic polymer was formed with a low content of hydrophobic groups in the main chains, which possessed a spatial network structure. In aqueous solution, hydrophobic groups got together because of hydrophobic flocculation, and the association reactions generated between intramolecular and intermolecular in the main chains. Even these reactions got much stronger in the brine solution because the addition of electrolytes increased the polarity of the solvent. Thus, the composite was a hydrophobic polymer with significant salinity resistance and thermostability. Combined with the previous performance, the collaboration of NBR and HM equipped the particle with good salt tolerance, excellent temperature resistance, and significant water-retention capability because of their thermostability and hydrophobic properties. Therefore, PMCP-4 was selected as the optimal particle.

Table VI. Properties of PMCP-4 under Different Conditions

Sample	Salinity (10^4 mg/L)	Temperature (°C)	Swelling ratio	P_{max} (MPa)	f
M1	0	100	15.79	0.13	1.00
M2	5.5		8.03	0.26	1.00
M3	11		7.10	0.39	0.98
M4	16.5		6.69	0.64	0.97
M5	22		6.45	0.82	0.94
M6	0	120	16.49	0.12	1.00
M7	5.5		8.01	0.28	1.00
M8	11		7.13	0.36	0.99
M9	16.5		6.81	0.54	0.98
M10	22		6.46	0.81	0.95

Toughness Assessment Experiment

With regard to the toughness of PMCP-4 under 100 and 120 °C, as shown in Table VI, two things were noted:

1. The high swelling ratio corresponded to a low strength and high toughness. This result could be interpreted as the fact that the intermolecular repulsion of the particle with a higher swelling ratio was more than that of their aggregation; this resulted in the relaxation of the molecular chains and caused the strength and toughness change.
2. Under the same temperature and salt concentration, PMCP-4 showed highest swelling ratio than the other three particles. Consequently, PMCP-4 was the toughest particle under high temperatures and salinities compared to the other three particles, and all of the *f*s were greater than 0.9. As expected, NBR was able to enhance the toughness of the particle on the basis of early study.[36] Therefore, PMCP-4 withstood mechanical shear in the fractured reservoirs because of its significant toughness and strength.

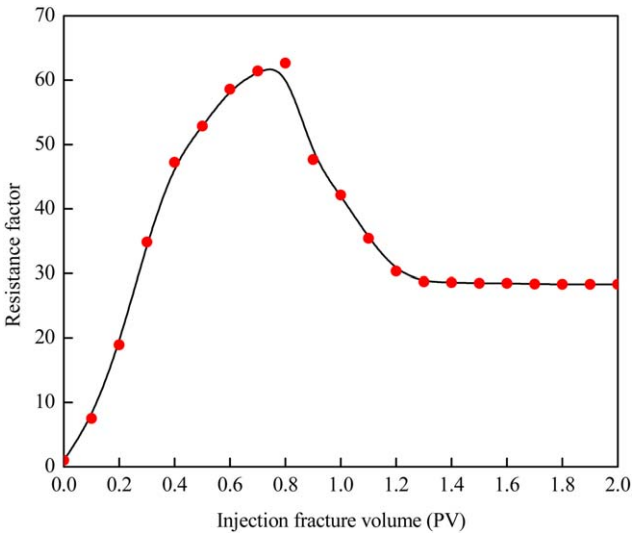

Figure 10. R_F as a function of the injection fracture volume. [Color figure can be viewed in the online issue, which is available at wileyonlinelibrary.com.]

Core Experiment

Single-Core Experiment. The R_F variation during particle injection as function of the fracture volume (PV) is plotted in Figure 10. It was interesting to see that R_F first increased with the particle suspension PV until a maximum value of 62.67 was reached at 0.8PV; in this process, the breakthrough pressure of the particle was 7.52 MPa. Then, R_F was followed by a sudden decrease and finally tended to stabilize at 28. This phenomenon could be explained as follows: the size of the particle was initially bigger than that of the fracture; this hindered the particle entrance into the core and made the pressure difference keep increasing until the breakthrough pressure was reached because of the elastic deformation and migration of the particles. After that, the pressure difference began to decrease and then tended to be stable when the particle suspension reached a steady flow.

We also observed from the core flow test that the particle transported along the fracture channel and was produced in the collector; this indicated that the particle had superior injection and transmission performance. Moreover, the particle at the effluent showed good performance of steady flow.

Double-Parallel-Core Physical Simulation Experiment. Two groups of cores were set up for the double-parallel-core experiment; these had permeability contrast values of 6.08 and 9.03, respectively. The results of profile control effect are shown in Table III; it was clear that the water absorption in the high-permeability fractures were 87 and 93% before profile control. However, after treatment with the particle, the values were decreased to 15 and 10%; this indicated the profile control ability of the particles. In addition, the particle showed a good selective injection; more particles (0.88 and 0.96PV) entered the high-permeability fractures. This made the fluid flow to low-permeability fractures and thus improved the water absorption in the low-permeability fractures (85 and 90%). The larger the permeability contrast value was, the better the profile improvement rate was. As expected, a significantly high profile improvement rate of more than 97% was obtained. The selective injection ability and high-quality profile improvement of the PMCP-4 had an excellent effect on the profile control for such fractured reservoirs.

CONCLUSIONS

After the introduction of rubbers and HM into PMCP, a promising profile control agent for water treatment in high-temperature and high-salinity fractured reservoirs was produced. On the basis of the experimental finding, some main conclusions could be drawn:

1. PMCP was successfully synthesized by *in situ* intercalative polymerization method. XRD characterization showed that the MMT interlayer spacing expanded by 0.5–0.6 nm; this manifested the accomplishment of the intercalation compound to PMCP.
2. HM and NBR were optimal materials for the preparation of desirable particles for their hydrophobic properties and thermostability. The optimum sample, PMCP-4, showed a swelling ratio 6.5 times greater at 120 °C and 220,000 mg/L. This

particle possessed characteristics as follows: tolerance to high temperature and salinity and high water-retention capacity.

3. PMCP-4 showed superior toughness at high temperatures and high salinities, and all the *f*s were greater than 0.9. It also exhibited good shear resistance in fractured reservoirs because of its toughness and strength.
4. The core experiments proved that the PMCP-4 had a good injectivity and high-quality profile control, and a high profile improvement rate of more than 97% was obtained. Therefore, PMCP-4 could selectively enter the high-permeability fractures and deeply migrate to modify the water absorption profile. Simultaneously, the water absorption was increased in low-permeability fractures. PMCP-4 would be advantageous for the deep profile control of high-temperature and high-salinity fractured reservoirs.

ACKNOWLEDGMENTS

The authors are grateful to the Scientific Research Project of Education Office in Sichuan Province (14ZB0042) for its financial support of this work.

REFERENCES

1. Zhang, H.; Bai, B. J. *SPE J.* **2011**, *16*, 388.
2. Lockhart, T. P. *SPE Adv. Technol.* **1994**, *2*, 199.
3. Jain, R.; McCool, C. S.; Green, D. W.; Willhite, G. P.; Michnick, M. J. *SPE J.* **2005**, *10*, 247.
4. Jia, H.; Pu, W. F.; Zhao, J. Z.; Jin, F. Y. *Ind. Eng. Chem. Res.* **2010**, *49*, 9618.
5. Jia, H.; Pu, W. F.; Zhao, J. Z.; Liao, R. *Energy Fuel* **2011**, *25*, 727.
6. Wei, B. J. *Appl. Polym. Sci.* **2015**, *132*, 10.
7. Hitzman, D. O.; Dennis, M.; Hitzman, D. C.; Hitzman, D. O.; Dennis, M.; Hitzman, D. C. Presented at SPE/DOE Symposium on Improved Oil Recovery, April **2004**, Tulsa, Oklahoma.
8. Strappa, L. A.; Lucia, J. P.; Maure, M. A.; Llopiz, M. L.; Strappa, L. A.; Lucia, J. P. Presented at SPE/DOE Symposium on Improved Oil Recovery, April **2004**, Tulsa, Oklahoma.
9. Willett, J. L.; Finkenstadt, V. L. J. *Polym. Environ.* **2006**, *14*, 2.
10. Nakason, C.; Wohmang, T.; Kaesaman, A.; Kiatkamjornwong, S. *Carbohydr. Polym.* **2010**, *81*, 2.
11. Mostafa, K. M. *J. Appl. Polym. Sci.* **1995**, *56*, 263.
12. Bai, B. J.; Liu, W.; Liang-Xiong, L. I.; Liu, G. H.; Tang, X. F. *Pet. Explor. Dev.* **2002**, *2*, 103.
13. Bai, B. J.; Li, L. X.; Liu, Y. Z.; Liu, H.; Wang, Z. G.; You, C. M. *SPE Reserv. Eval. Eng.* **2007**, *10*, 415.
14. Bai, B. J.; Liu, Y. Z.; Coste, J. P. *SPE Reserv. Eval. Eng.* **2007**, *10*, 176.
15. Delshad, M.; Varavei, A.; Goudarzi, A.; Zhang, H.; Sepehrnoori, K.; Bai, B.; Hu, Y. Presented at the SPE Western Regional & AAPG Pacific Section Meeting 2013 Joint Technical Conference, April, Monterey, CA; Paper No. SPE165356-MS.
16. Sang, Q.; Li, Y.; Yu, L.; Li, Z.; Dong, M. *Fuel* **2014**, *136*, 295.
17. Kytai, T. N.; West, J. L. *Biomaterials* **2002**, *23*, 22.
18. Wen, F. L.; Sung, C. L. *J. Appl. Polym. Sci.* **2006**, *100*.
19. Bai, B. J. Presented at the SPE Symposium on Improved Oil Recovery, April **2008**, Tulsa, OK; Paper No. SPE 113997.
20. Lv, X.; Hou, J. R.; Yue, X. A.; Cen, Q. S. *Sci. Technol. Ed.* **2010**, *32*, 143.
21. Xu, J.; Ke, Y.; Zhou, Q.; Hu, X.; Tan, Z.; Yang, L.; Zhang, G. *Polym. Compos.* **2014**, *356*, 1104.
22. Erol, O.; Unal, H. I.; Sari, B. *Polym. Compos.* **2010**, *31*, 471.
23. Ma, J.; Xu, J.; Ren, J. H.; Yu, Z. Z.; Mai, Y. W. *Polymer* **2003**, *44*, 4619.
24. Vaia, R. A.; Ishii, H.; Giannelis, E. P. *Chem. Mater.* **1993**, *5*, 1694.
25. Tongwa, P.; Bai, B. *J. Pet. Sci. Eng.* **2014**, *124*.
26. Zhu, Z.; Jian, O.; Paillet, S.; Desbrières, J.; Grassl, B. *Eur. Polym. J.* **2007**, *43*, 3.
27. Guo, H. P.; Gao, B. J.; Zhang, Y.; Wang, J. J. *Funct. Polym.* **2008**, *21*, 2.
28. Lv, X.; Jing, Y.; Zheng, Y. *Adv. Fine Petrochem.* **2003**, *4*, 9.
29. Jiang, F.; Pu, W.; Li, Y.; Du, D. *Photochem. Photobiol.* **2015**, *132*, 38.
30. Ma, H. W.; Liu, Y. Z.; Li, Y. K.; Xiong, C. M.; Li, Z. Y.; Li, C. X.; Tian, J. R. *Pet. Explor. Dev.* **2008**, *35*, 6.
31. Zhao, X. T.; Dong, L. Y.; Fu, M. J.; Tang, J. Y. *Pet. Geol. Rec. Eff.* **2014**, *21*, 6.
32. Wang, C. Q.; Zhang, G.; Dong, Y. P.; Chen, X. F.; Tan, H. M. J. *Appl. Polym. Sci.* **2002**, *86*, 12.
33. Dehbari, N.; Zhao, J. C.; Peng, R. G.; Tang, Y. H. J. *Mater. Sci.* **2015**, *50*, 15.
34. Gao, L. M.S. Thesis, Hunan University, **2008**.
35. Zhang, Y. Thesis, China University of Petroleum (East China), **2013**.
36. Pu, W. F.; Wen, C. L.; Liu, R.; Jin, F. Y.; Zhao, L.; Song, T. *Chem. Res. Appl.* **2015**, *8*, 1134.
37. Pu, W. F.; Liu, R.; Sun, L.; Yan, Z. P.; Shang, X. P.; Zhao, L. Chin. Pat. Appl. CN104327821A (**2015**).
38. Lee, S.; Park, Y. J. *Mater. Chem.* **2003**, *13*, 2942.
39. Pu, W. F.; Luo, X. B.; Wei, L. S. Water Plugging Technology of Dual Crosslinked Composite Gel in Low Permeability Fractured Reservoir; Petroleum Industry: Beijing, **2006**.
40. Okamoto, M.; Morita, S.; Kim, Y. H.; Kotaka, T.; Tateyama, H. *Polymer* **2001**, *42*, 1201.

SGML and CITI Use Only
DO NOT PRINT